Experimental and numerical analysis of mixed mode fracture

Octavian POP[1,*], Mamadou Méité[1], Frédéric Dubois[1], Joseph Absi[2]

[1] GEMH, Université de Limoges, Centre Universitaire de Génie Civil, 19300 Egletons
[2] GEMH, Université de Limoges, IUT du Limousin, Département GM, 87000 Limoges
* Corresponding author: ion-octavian.pop@unilim.fr

Abstract Based on the global approach and the experimental measurements by digital image correlation, the presented study proposes a coupling between these two approaches in order to evaluate energy release rate. The proposed formalism allows calculating the energy release rate fracture parameters without considering the elastic parameters of material. The experimental analysis is realized using the specimens made in PVC isotropic material and Douglas fir (orthotropic material) under different mixed mode loadings. The loading under displacement control is applied using the Arcan system. From experimental data optimized by an adjustment procedure, the kinematic state in the crack tip vicinity is evaluated through the crack opening relative displacement factors. In parallel the stress state in vicinity of the crack tip is evaluated by a numerical analysis. This analysis is performed using the finite elements method and the integral invariant Mtheta, in order to evaluate the stress intensity factors. The finite element analysis is based on the reproduction of experimental test in terms of specimen geometry, experimental boundaries conditions and loading configurations. Then the energy release rate can be estimated by coupling of these two factors calculated without considering the material elastic parameters. Moreover, this method allows defining the local mechanical behavior.

Keywords Fracture mechanics, Mixed Mode, Experimental, Numerical, Digital Image Correlation

1. Introduction

Cracked structures are most often subjected to complex loadings in mixed-mode configurations that can lead to a catastrophic collapse of the structure and modify their mechanical behavior. In this case in order to avoid structural behavior, it is necessary to evaluate fracture process parameters and local mechanical behavior. Within this field of study, several numerical investigations have been carried out in the literature for the purpose of characterizing crack tip parameters through use of the energy method for mixed-mode configurations [1-4], for isotropic and orthotropic media. At present, these efficient techniques require an explicit knowledge of material properties; for orthotropic cases in particular, the complete compliance tensor is needed. In this context, our study proposes a new formalism that allows uncoupling the fracture parameter identification relative to material elastic properties.

Based on Digital Image Correlation (DIC) and a Finite Element Method (FEM), the fracture parameter identification can be performed from the kinematic and stress distributions in the crack tip vicinity. The complementarity of these two approaches distinguishes the calculation of energy release rates relative to opening and shear modes from the calculation of local material elastic proprieties.

According to our approach, DIC is employed to measure the displacement field evolution for the specimens made from a rigid Polyvinyl Chloride polymer and Douglas fir loaded under mixed-mode configurations. The application of such an experimental technique enables capturing both strong and weak kinematic discontinuities in the crack tip vicinity so as to characterize Crack Relative Displacement Factor (CRDF) [5-9]. The iterative Newton-Raphson method is then coupled with DIC to provide not only the real crack tip position needed for an accurate CRDF determination, but also the comprehensive raw dataset optimized through Williams' asymptotic series expansion solution.

The evaluation of stress distribution is realized using a finite element model. The model is based on experimental sample geometry and experimental boundary conditions. According to the Mq method, Stress Intensity Factor (SIF) is defined by introducing a mixed-mode separation algorithm. For isotropic as for orthotropic configurations, stress distribution into the crack tip domain is assumed to be unaffected by elastic properties [5-7].

By aggregating the results of CRDF yielded by experimental DIC and SIF, as given by a numerical FEM, the prediction of an accurate energy release rate can be proposed. Fracture mode separation is also analyzed by establishing mode I and mode II energy release rates for mixed-mode loading conditions as well as plane configurations.

2. Experimental material and methods

The experimental evaluation of has been performed for several mixed-mode ratios. As shown in Figure 1, the experimental set-up involves an electromechanical press fitted with an LVDT displacement transducer and a load cell. The specimen geometry is a single-edge notched sample made from Polyvinyl Chloride (PVC) for the isotropic case and Douglas fir in the orthotropic case. The specimen dimensions are $208 \times 144 \times 10\,mm^3$ for the PVC specimen and $210 \times 150 \times 10\,mm^3$ with a notch length equal to $75\,mm$. The various mixed-mode loading configurations are applied thanks to Arcan fixtures that allow imposing a number of different mixed-mode ratios defined by the angle between force direction and crack orientation. The test is run under a displacement control with an imposed velocity of the cross-head equal to 0.1 mm/s.

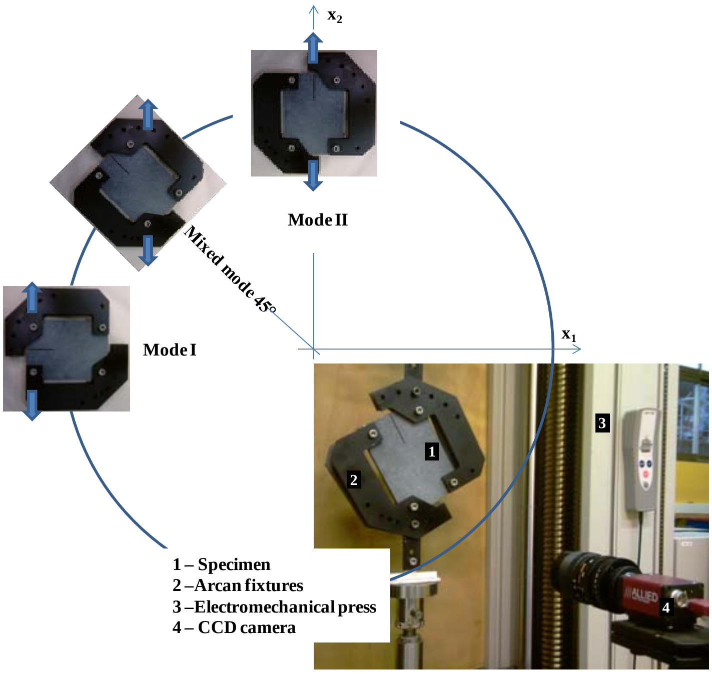

Figure 1. Experimental setup

Concerning measurement devices, the displacement field evolution is recorded on the specimen surface using an 8-bit CCD camera (1392×1040 pixel). The image capture is performed at a rate of 1 frame per second and synchronized with the electromechanical press data (force and displacement). According to the DIC principle, a black-and-white speckled pattern is projected onto the specimen surface [10, 11]. The principle of this full-field method is based on a comparison between two images acquired during the test, one before deformation and the other after. The displacement field can then be obtained by comparing the reference image with the deformed image [10, 11]. The displacement fields, as presented in the present paper, are limited to 2D measurements. 3D effects are neglected (out-of-plane of crack lips or shear buckling induced by the specimen thickness), and plane stress state has been assumed.

2.1. Crack Relative Displacement Factor evaluation from experimental measurement

The experimental evaluation of CRDFs has been performed from the experimental measurements by DIC. The displacement data output by the DIC method are typically affected by experimental noise. It proves quite difficult to accurately analyze stress and strain fields from raw displacement data; moreover, real deformation fields of the crack tip and its location are difficult to obtain with precision from DIC [5-7, 11-14]. Consequently, the crack tip parameters predicted directly using raw experimental displacement data are inaccurate [5-7]. An adjustment procedure has thus been derived to avoid these difficulties.

Then, once the experimental displacement has been calculated, the adjustment procedure based on a nonlinear iterative Newton-Raphson is performed between the Williams' series forms (1) and the experimental data. By taking measurement boundary conditions (e.g. specimen geometry and symmetry, crack orientation) into account, this adjustment procedure is also able to consider a rigid body motion, crack tip localization and its orientation as unknowns. These parameters are then used to adjust the displacement fields.

$$
\begin{aligned}
u^1 &= \sum_{c=1}^{N} \left[A_1^c \cdot r^{(c/2)} \, f_c(\kappa,\varphi) + A_2^c \cdot r^{(c/2)} \, g_c(\kappa,\varphi) \right] + T_1 - R \cdot x_2 \\
u^2 &= \sum_{c=1}^{N} \left[A_1^c \cdot r^{(c/2)} \, l_c(\kappa,\varphi) + A_2^c \cdot r^{(c/2)} \, z_c(\kappa,\varphi) \right] + T_2 + R \cdot x_1
\end{aligned}
\tag{1}
$$

Where:

$$
\begin{aligned}
f_c &= \kappa \cdot \cos\left(\frac{c}{2}\varphi\right) - \frac{c}{2} \cdot \cos\left(\left(\frac{c}{2}-2\right)\varphi\right) + \left((-1)^c + \frac{c}{2}\right)\cos\left(\frac{c}{2}\varphi\right) \\
g_c &= (-1) \cdot \kappa \sin\left(\frac{c}{2}\varphi\right) - \frac{c}{2} \cdot \sin\left(\left(\frac{c}{2}-2\right)\varphi\right) + \left((-1)^c - \frac{c}{2}\right)\sin\left(\frac{c}{2}\varphi\right) \\
l_c &= \kappa \cdot \sin\left(\frac{c}{2}\varphi\right) + \frac{c}{2} \cdot \sin\left(\left(\frac{c}{2}-2\right)\varphi\right) - \left(\frac{c}{2} + (-1)^c\right)\sin\left(\frac{c}{2}\varphi\right) \\
z_c &= \kappa \cdot \cos\left(\frac{c}{2}\varphi\right) + \frac{c}{2} \cdot \cos\left(\left(\frac{c}{2}-2\right)\varphi\right) + \left(\frac{c}{2} - (-1)^c\right)\cos\left(\frac{c}{2}\varphi\right)
\end{aligned}
\tag{2}
$$

The adjusted experimental field now allows defining a physical and local interpretation. The kinematic state of crack lips can in fact be identified using Crack Relative Displacement Factor $K_{\alpha}^{(e)}$ (CRDF) [5-9], which denote the relative opening and shear displacements of crack lips. Thanks to developments offered by Dubois, the kinematic state in the crack tip vicinity can be defined using Crack Relative Displacement Factors (CRDFs). At a very short distance x from the crack tip, the relative opening displacement $[u]_1$ and shear displacement $[u]_2$ are defined as follows (see Figure 2):

$$
[\![u]\!]_1 = K_2^{(e)} \cdot \sqrt{\frac{x}{2\cdot\pi}} \quad and \quad [\![u]\!]_2 = K_1^{(e)} \cdot \sqrt{\frac{x}{2\pi}} \tag{3}
$$

By combining Eqs. (1) with (3), we can now provide, in the crack tip vicinity, a mathematical interpretation of CRDF, such that:

$$
K_1^{(e)} = 2 \cdot A_1^1 \, (\kappa + 1) \cdot \sqrt{2\pi} \quad and \quad K_2^{(e)} = 2 \cdot A_2^1 \, (\kappa + 1) \cdot \sqrt{2\pi} \tag{4}
$$

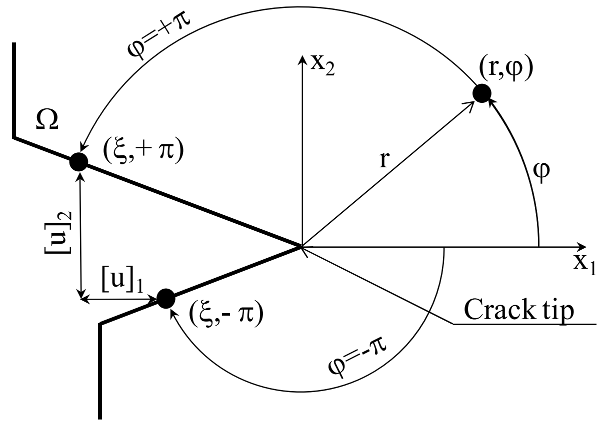

Figure 2. Relative displacements of crack lips

In Eqs. (1), (2), (3) and (4), (r, j) are the polar coordinates, k is the constant of Kolossov, A_a^c are the weighting coefficients relative to opening mode (α=1) and shear mode (α=2) and (T_1, T_2, R) are the rigid body motions.

From Eqs. (4), the CRDF can be determined without an explicit knowledge of the material elastic properties. Moreover, this initial step aims to accurately characterize the kinematic state of the crack.

2.2. Stress Intensity Factor evaluation from numerical analysis

In fracture mechanics, the stress state definition in the crack vicinity is expressed in terms of Stress Intensity Factor (SIF) $K_a^{(s)}$. As previously mentioned, the experimental test is conducted under displacement control, while the numerical model is loaded by imposing an equivalent force. In this case, SIF amplitude depends solely on model geometry, crack length and the force loading value.
The definition of these factors implies developing a classical finite element model (Figure 3).

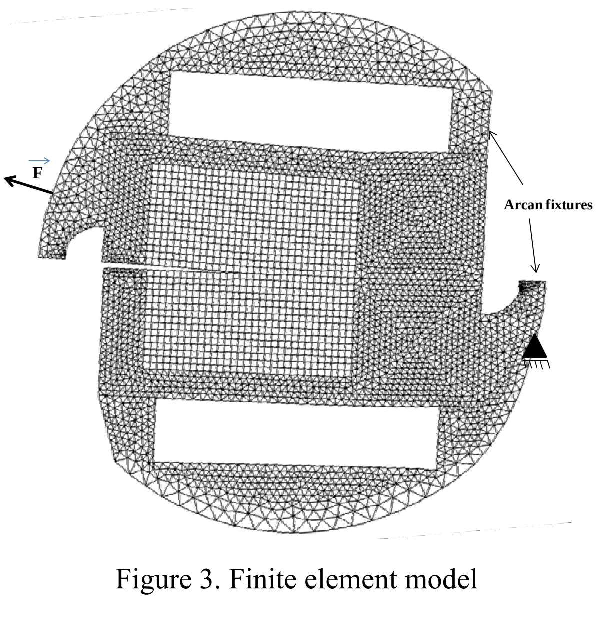

Figure 3. Finite element model

Note that the boundary conditions implemented in the finite element model have not integrated the experimental flaws, in terms of rigid body motion and crack tip orientation. Let's recall that these parameters have already been integrated into the optimized displacement fields obtained from the adjustment procedure described above. According to the finite element approach, we therefore place ourselves in an "ideal" test configuration.

In mixed-mode configurations, SIF calculations are often performed by implementing $M\theta$ method (Figure 4). The $M\theta$-integral is an energy parameter established in order to analyze crack growth in a mixed-mode fracture by isolating various fracture modes, such as opening and shear, through a pseudo-potential that combines real displacements and kinematically admissible auxiliary displacements.

$$M\theta = \frac{1}{2} \cdot \int_V \left(\left(\sigma_{ij}\right)_{real} \cdot \left(u_{i,k}\right)_{aux} - \left(\sigma_{ij,k}\right)_{aux} \cdot \left(u_i\right)_{real} \right) \cdot \theta_{k,j} \cdot dV \tag{5}$$

The relationships between the stress tensor and the displacement vectors require introducing orthotropic elastic properties. By imposing an external force loading however, we can assume that SIF are not really influenced by elastic properties. Given these conditions, we have opted for an arbitrary elastic property rated '~'.

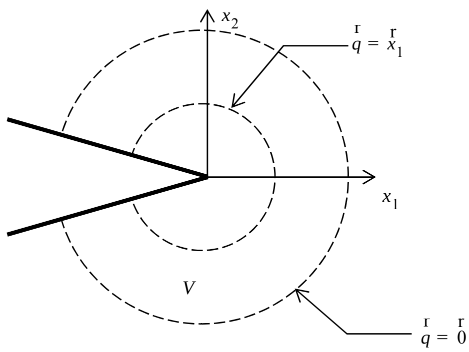

Figure 4. Integral domain

2.3. New formalism of energy release rate

The coupling between the kinematic and stress approaches allows calculating an energy release rate by the surrounding elastic proprieties. This coupling also serves to identify the actual reduced elastic compliance leading to the Young's modulus determination. Now, by replacing virtual displacements by real displacements, it has been shown that the $M\theta$ integral is mistaken for the energy release rate G [15]. More precisely, thanks to the superposition principle, in letting ${}^{real}K_\alpha^{(s)}$ and ${}^{aux}K_\alpha^{(s)}$ be the real and virtual Stress Intensity Factor, respectively, we can adopt the following expression:

$$M\theta(\vec{u},\vec{v}) = \sum_\alpha C_\alpha \cdot \frac{{}^{real}K_\alpha^s \cdot {}^{aux}K_\alpha^s}{8} \tag{6}$$

where C_α is the reduced elastic compliance that allows defining local behavior in terms of Stress

Intensity Factor and Crack Relative Displacement Factor, such that:

$$K_{\alpha}^{\varepsilon} = C_{\alpha} \cdot {}^{real}K_{\alpha}^{\sigma} \qquad (7)$$

Equation (6) yields a physical interpretation for Mq in the Stress Intensity Factor definition, i.e.:

$${}^{u}K_{1}^{(s)} = \frac{8 \cdot Mq\left(K_{1}^{(s)} = 1,\ {}^{v}K_{2}^{(s)} = 0\right)}{C_{1}} \ \ and \ \ {}^{u}K_{2}^{(s)} = \frac{8 \cdot Mq\left(K_{1}^{(s)} = 0,\ {}^{v}K_{2}^{(s)} = 1\right)}{C_{2}} \qquad (8)$$

For orthotropic media, these arbitrary reduced elastic compliance functions are defined by the following equations:

$$\tilde{C}_{1} = \sqrt{\frac{\tilde{a}_{11}\,\tilde{a}_{22}}{2}} \cdot \sqrt{\sqrt{\frac{\tilde{a}_{22}}{\tilde{a}_{11}}} + \frac{2\,\tilde{a}_{12} + \tilde{a}_{33}}{2\,\tilde{a}_{11}}} \ \ and \ \ \tilde{C}_{2} = \sqrt{\frac{\tilde{a}_{11}\,\tilde{a}_{11}}{2}} \cdot \sqrt{\sqrt{\frac{\tilde{a}_{22}}{\tilde{a}_{11}}} + \frac{2\,\tilde{a}_{12} + \tilde{a}_{33}}{2\,\tilde{a}_{11}}} \qquad (9)$$

Where:

$$\tilde{a}_{11} = \frac{1}{\tilde{E}_{L}};\ \tilde{a}_{12} = -\frac{\tilde{\nu}_{RL}}{\tilde{E}_{R}} = -\frac{\tilde{\nu}_{LR}}{\tilde{E}_{L}};\ \tilde{a}_{22} = \frac{1}{\tilde{E}_{R}};\ \tilde{a}_{33} = \frac{1}{\tilde{G}_{LR}} \quad \text{in plane stress} \qquad (10)$$

$$\tilde{a}_{11} = \frac{1 - \tilde{\nu}_{LT} \cdot \tilde{\nu}_{TL}}{\tilde{E}_{L}};\ a_{12} = -\frac{\tilde{\nu}_{RL}\ \ \tilde{\nu}_{RL} \cdot \tilde{\nu}_{TL}}{\tilde{E}_{R}};\ a_{22} = \frac{1\ \ \tilde{\nu}_{RT} \cdot \tilde{\nu}_{TR}}{\tilde{E}_{R}};\ \tilde{a}_{33} = \frac{1}{\tilde{G}_{LR}} \quad \text{in plane strain} \qquad (11)$$

In which $\tilde{E}$ and $\tilde{\nu}$ are the arbitrary elastic orthotropic properties of material.

In the case of isotropic material the arbitrary reduced elastic compliance functions are defined by:

$$\tilde{C}_{a} = \frac{\tilde{k} + 1}{\tilde{m}} \qquad (12)$$

Where m is the Lamé coefficient given by :

$$\tilde{m} = \frac{\tilde{E}}{2 \cdot \left(1\ \ \tilde{n}\right)} \qquad (13)$$

And:

$$k = 3 - 4 \cdot n \ \ in\ \ plane\ strain$$

$$k = \frac{3 - n}{1 + n} \ \ in\ \ plane\ stress \qquad (14)$$

Now, in assuming a plane stress state, by substituting Equation (7) into the classical energy release rate expression, we obtain a new formalism:

$$G_{a} = \frac{{}^{real}K_{a}^{(s)} \times K_{a}^{(e)}}{8} \qquad a = 1;2 \qquad (15)$$

In Eq. (15) G_{α} represents the portion of opening and shear modes in terms of energy release rate.

Next, using the numerical values of CRDFs and SIFs calculated above, the energy release rate can be estimated from Equation (15) independently of the material's elastic proprieties.

3. Results

In the case of rigid Polyvinyl Chloride polymer and Douglas fir the Figure 5 highlights a comparison between the experimental and analytical deformations after adjustment procedure.

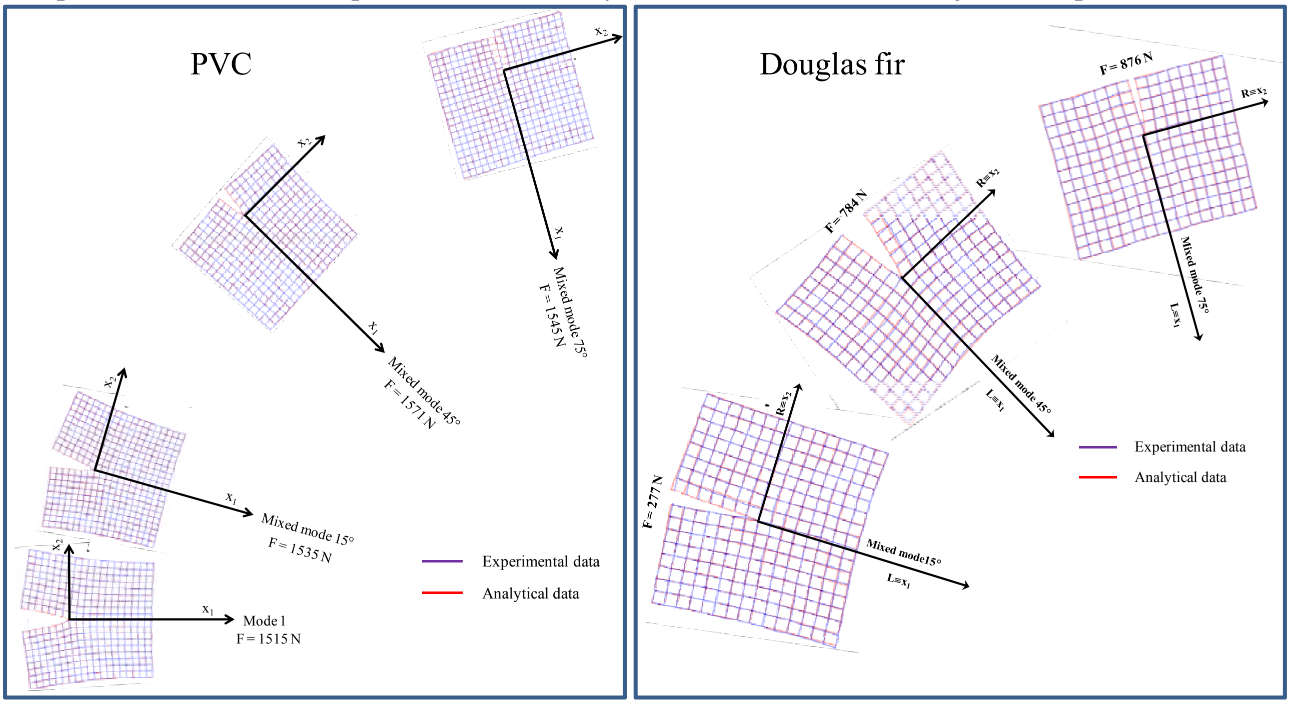

Figure 5. Results of the adjustment procedure

As is shown in Figure 5, the adjustment procedure allows obtaining an optimized displacement fields without experimental noises. Moreover, the adjustment procedure allows estimating the rigid body motion and the crack tip orientation. These parameters are essential to adjust the experimental conditions in order to obtain the specific mixed mode boundary conditions definite by the analytical expressions of displacement fields corresponding to mixed mode loading. Note that the representation of displacements fields shown in Figure 5 take into account these parameters.

According to Equations (4), the $K_a^{(e)}$ values are calculated from optimized displacement fields using the values of A_1^1, A_2^1 and k values. Then the Stress Intensity Factor can be evaluated from a FE analysis via the integral invariant Mq.

According to Equation (15), the energy release rate can be predicted by combining a kinematic approach (given by experimental testing) with a static approach (using numerical modeling) through determining CRDF and real SIF, respectively. The results of these energy release rate predictions are provided in Table 1 for isotropic case and Table 2 for orthotropic case. Not only does this method allow deducing the energy release rate, but moreover the use of the Mq-integral allows separating this energy for each part of both the opening and shear modes.

Table 1: Isotropic case

b	Force (N)	$K_1^{(\varepsilon)}$ ($m^{1/2}$)	$K_2^{(\varepsilon)}$ ($m^{1/2}$)	$K_1^{(\sigma)}$ ($MPa \cdot m^{1/2}$)	$K_2^{(\sigma)}$ ($MPa \cdot m^{1/2}$)	G_1 (J/m^2)	G_2 (J/m^2)
0°	1515	$5.03 \cdot 10^{-3}$	0	1.63	0	1025	0
15°	1535	$2.04 \cdot 10^{-3}$	$3.44 \cdot 10^{-4}$	0.66	0.11	168	5
45°	1571	$2.34 \cdot 10^{-3}$	$9.80 \cdot 10^{-4}$	0.76	0.32	222	39
75°	1545	$5.49 \cdot 10^{-4}$	$9.51 \cdot 10^{-4}$	0.18	0.31	10	37

Table 2: Orthotropic case

b	Force (N)	$K_1^{(\varepsilon)}$ ($m^{1/2}$)	$K_2^{(\varepsilon)}$ ($m^{1/2}$)	$K_1^{(\sigma)}$ ($MPa \cdot m^{1/2}$)	$K_2^{(\sigma)}$ ($MPa \cdot m^{1/2}$)	G_1 (J/m^2)	G_2 (J/m^2)
0°	245	$2.08 \cdot 10^{-3}$	0	0.45	0	116	0
15°	277	$5.95 \cdot 10^{-4}$	$1.43 \cdot 10^{-4}$	0.14	0.11	10.5	2.02
45°	748	$1.35 \cdot 10^{-3}$	$7.43 \cdot 10^{-4}$	0.32	0.59	54	55.2
75°	876	$6.91 \cdot 10^{-4}$	$6.58 \cdot 10^{-4}$	0.16	0.52	14.2	42.9

4. Conclusion

This work has presented an original coupling between Digital Image Correlation and Finite Element Analysis, making it possible to characterize both the mechanical and energy states in the crack tip vicinity.
Based on Dubois' developments, the kinematic state in the crack tip vicinity is evaluated using the Crack Relative Displacement Factors calculated from experimental measurements output by DIC. In parallel with this step, the stress distribution is evaluated by a finite element analysis according to the Mq method. The coupling of these two approaches allows distinguishing and calculating the energy release rates corresponding to opening and shear modes. The originality of this coupling procedure lies in the possibility of calculating the energy release rate independently of material elastic properties. Furthermore, our formalism allows evaluating local elastic properties via the elastic compliance correlated with Crack Relative Displacement Factors and Stress Intensity Factors.
In terms of follow-up work, crack initiation and propagation can be studied in greater depth thanks to this new technique, thus leading to a better understanding of all phenomena governing the crack tip growth process.

References

[1] B. Budiansky, J.R Rice, Conservation laws and energy release rate. Journal of Applied Mechanics, 400 (1973) 201-203.
[2] A.G. Hermann, On energy release rates for a plane crack. Journal of Applied Mechanics, 48, (1981) 525-528.
[3] L.B. Freund, Stress-intensity factor calculations based on a conservation integral. International of Journal of Solids and Structures, 14 (1978) 241-250.
[4] J.H. Chang, A.J. Chien, Evaluation of M-integral for anisotropic elastic media with multiple

defects. International Journal of Fracture, 114 (2002) 267-289.

[5] F. Dubois, M. Méité, O. Pop, J. Absi, Characterization of timber fracture using the Digital Image Correlation technique and Finite Element Method. Engineering Fracture Mechanics (2012). doi.org/10.1016/j.engfracmech.2012.07.008.
[6] O. Pop, M. Meite, F. Dubois, J. Absi, Identification algorithm for fracture parameters by combining DIC and FEM approaches. International Journal of Fracture, 170 (2011) 101-114.
[7] M. Méité, O. Pop, F. Dubois, J. Absi, Characterization of mixed-mode fracture based on a complementary analysis by means of full-field optical and finite element approaches. International Journal Fracture, (2012). DOI: 10.1007/s10704-012-9794-z.
[8] F. Dubois, C. Chazal, C. Petit, Viscoelastic crack growth process in wood timbers: an approach by the finite element method for mode I fracture. International Journal Fracture; 113 (2002) 367–88.
[9] F. Dubois, C. Petit, Modeling of the crack growth initiation in viscoelastic media by the Gθ integral. Engineering Fracture Mechanics, 72 (2005) 2821–2836.
[10] M.A. Sutton, W.J. Wolters, W.H. Peters, W.F. Ranson, S.R. McNeil, Determination of Displacements Using an Improved Digital Correlation Method, Image and Vision Computating, 1 (1983) 133-139.
[11] J. Réthoré, S. Roux, F. Hild, Optimal and noise-robust extraction of Fracture Mechanics parameters from kinematic measurements. Engineering Fracture Mechanics 78 (2011) 1827-1845.
[12] K. Machida, Y. Suzuki, Examination of the accuracy of the singular stress fields near a crack tip by Digital Image Correlation. Key Engineering Materials, 321 (2006) 32–37.
[13] S. Yoneyama, T. Ogawa, Y. Kobayashi, Evaluating mixed-mode stress intensity factors from full-field displacement obtained by optical methods. Engineering fracture mechanics, 74 (2007) 1399–1412.
[14] M. Méité, O. Pop, F. Dubois, J. Absi, Evaluation of mixed-mode integral invariant for polymer material trough the couple experimental-numerical Process. 14th International Conference on Experimental Mechanics (ICEM14), Poitiers, 2010.
[15] R. Moutou Pitti, F. Dubois, C. Petit, N. Sauvat, Mixed mode fracture separation in viscoelastic orthotropic media: numerical and analytical approach by the Mθv –integral. International Journal of Fracture, 145 (1997) 181–193.